Karlsruhe Institute of Technology

Elektrotechnisches Institut (ETI)
Prof. Dr.-Ing. Michael Braun
Prof. Dr.-Ing. Martin Doppelbauer
Prof. Dr.-Ing. Marc Hiller
Kaiserstr.12. 76131 Karlsruhe

Elektrotechnisches Institut

Title:	Operating Performance of the Modular Multilevel Matrix Converter in Drive Applications
Authors:	Felix Kammerer, Dennis Bräckle, Mario Gommeringer, Mathias Schnarrenberger, Michael Braun
Institute:	Karlsruhe Institute of Technology (KIT) Elektrotechnisches Institut (ETI)
Type:	Conference Proceedings of the PCIM Europe 2015 (www.pcim-europe.com)
Published at:	Proceedings 2015 PCIM Europe, International Conference and Exhibition for Power Electronics, Intelligent Motion, Renewable Energy and Energy Management, Nuremberg, Germany, May 19-21, 2015 Publisher: VDE Verlag Year: 2015 ISBN: 978-3-8007-3924-0 Pages: 549-556
Hyperlinks:	http://ieeexplore.ieee.org/xpl/articleDetails.jsp?arnumber=7149076

Operating Performance of the Modular Multilevel Matrix Converter in Drive Applications

Felix Kammerer, Dennis Bräckle, Mario Gommeringer, Mathias Schnarrenberger, Michael Braun
Elektrotechnisches Institut (ETI) - Electrical Drives and Power Electronics
Karlsruhe Institute of Technology (KIT), Kaiserstr. 12, 76131 Karlsruhe, Germany
Tel.: +49 721 608 42461, E-mail: felix.kammerer@kit.edu

Abstract

The Modular Multilevel Matrix Converter (M3C) is an emerging topology, especially suitable for high torque low speed drive applications in the medium voltage range. One special benefit is the overload capability of the output currents. Up to 200% of the nominal values can be reached near standstill to overcome breakaway torques without additional efforts. This contribution gives an experimental verification of the operating performance by using a low voltage laboratory prototype with 5 cells per arm. In addition, different energy balancing methods, depending on the operating point are presented. Finally, possible applications for the M3C are discussed.

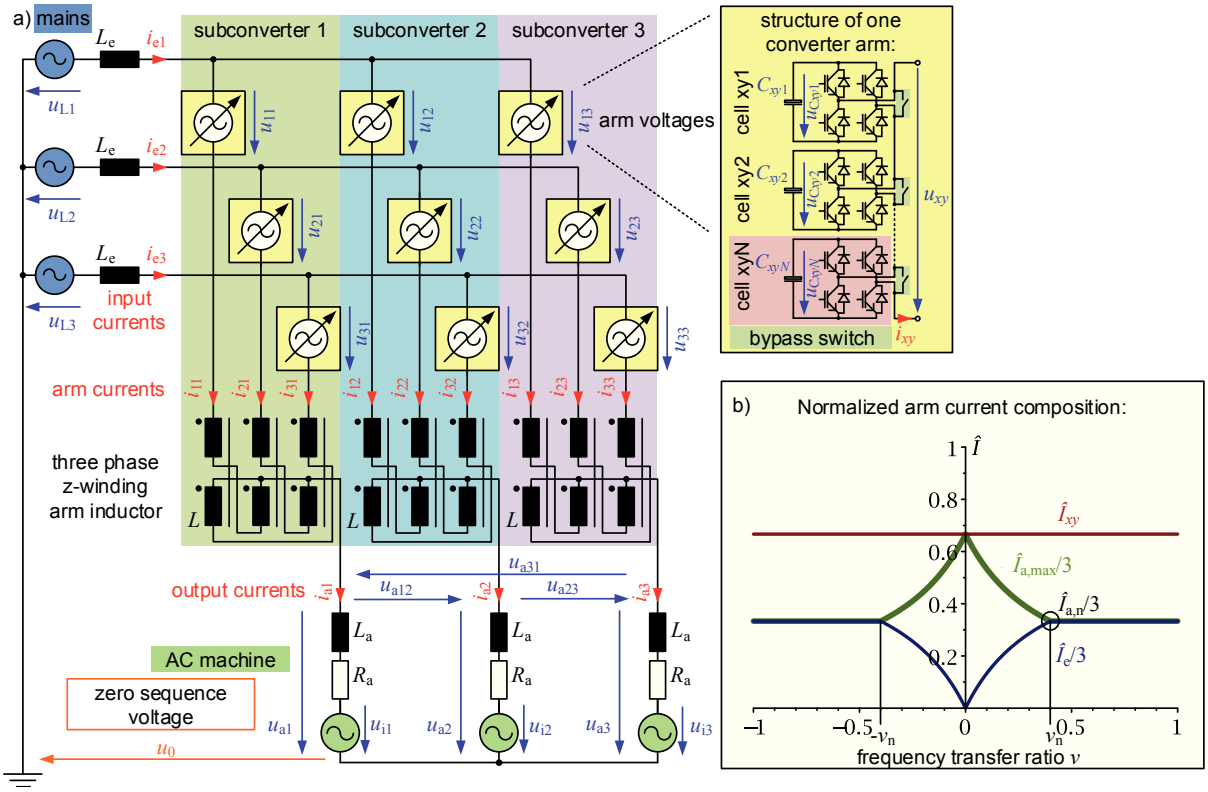

Fig. 1: a) Modular Multilevel Matrix Converter (M3C) for feeding high torque variable speed drives. The nine M3C converter arms consist of N series connected H-bridges with a DC-capacitor C_{xyz}.
b) Normalized arm current composition for an M3C feeding a 3AC machine ($\cos(\varphi_\mathrm{a}) = 1$) with a nominal output current amplitude of $\hat{I}_\mathrm{a,n} = 1$. The maximum arm current $\hat{I}_{xy}$ is held constant in the whole speed range. At low speeds the output current amplitude $\hat{I}_\mathrm{a,max}$ can be increased up to 200% of the nominal value $\hat{I}_\mathrm{a,n}$ to generate a higher torque [1].

1. Introduction

The Modular Multilevel Matrix Converter (M3C), shown in Fig. 1a), performs a direct 3AC to 3AC power conversion. It is particularly suitable for high voltage drive applications that require low nominal frequencies. The M3C can be used to replace line commutated cycloconverters due to its modular and scalable structure. Its high voltage quality on the input and output side avoids expensive filters. High reliability requirements can be fulfilled with the M3C by installing bypass switches (see Fig. 1a)). In case of cell failures the corresponding bypass switches are closed and the operation continues with a reduced number of cells.

In the first part of this paper the output current overload capability and the energy balancing of the M3C is explained. Subsequently the low voltage laboratory prototype is presented and measurement results show the operating performance of the M3C for feeding 3AC machines. In the last part possible applications for the M3C are discussed.

2. Output current overload capability of the M3C

The overall system including the three-phase AC grid, the Modular Multilevel Matrix Converter (M3C) and the three-phase machine is shown in Fig. 1a). The nine converter arms are modeled as controllable voltage sources and consist of N series connected cells. They are realized as H-bridges with a capacitor C_{xyz} (x = input phase number, y = output phase number, $x, y \in \{1, 2, 3\}$, z = cell number, $z \in \{\mathbb{N} | 1 \leq z \leq N\}$). By switching the transistors of the cells, each arm is able to generate an adjustable arm voltage u_{xy} with $2N + 1$ voltage steps. The nine arm currents i_{xy} can be described as four space vectors with their corresponding $\alpha\beta$-components. The detailed calculations are given in [2]. Fig. 2 shows the four space vectors with the corresponding phase components marked in red, blue and green. The distribution of the phase components along the nine converter arms is given in the lower part of Fig. 2. The nine arm currents i_{xy} can be calculated by adding the phase components of the four space vectors according to the colors given in Fig. 2. For example, the arm current i_{11} contains the following space vector components:

$$i_{11} = \frac{i_{\mathrm{e1}}}{3} + \frac{i_{\mathrm{a1}}}{3} + i_{\mathrm{d11}} + i_{\mathrm{d21}} \tag{1}$$

The maximum arm current $\hat{I}_{xy}$ is the dimensioning criteria for the current capability of the semiconductors and cell capacitors C_{xyz}. With (1) and assuming sinusoidal currents, it can be calculated to [1]:

$$\hat{I}_{xy} = \frac{\hat{I}_{\mathrm{e}}}{3} + \frac{\hat{I}_{\mathrm{a}}}{3} + \hat{I}_{\mathrm{d1}} + \hat{I}_{\mathrm{d2}} \tag{2}$$

Equation (2) contains four different components. This feature can be used in drive applications to generate a higher output current and therefore a higher torque at low speeds [1]. This is possible due to the fact that the active output power P_{a} and therefore the input currents i_{ex} are low at low speeds. The remaining arm current capability can be used to generate a higher output current in this operation area. The maximum output current amplitude $\hat{I}_{\mathrm{a,max}}$ can be calculated for a given arm current $\hat{I}_{xy}$. Here the losses and the internal diagonal currents i_{d1} and i_{d2} are neglected due to their low values at steady state operation [1]:

$$\hat{I}_{\mathrm{a,max}} = \frac{3 \cdot \hat{I}_{xy}}{1 + \frac{\hat{U}_{\mathrm{a}} \cdot \cos(\varphi_{\mathrm{a}})}{\hat{U}_{\mathrm{e}} \cdot \cos(\varphi_{\mathrm{e}})}} \tag{3}$$

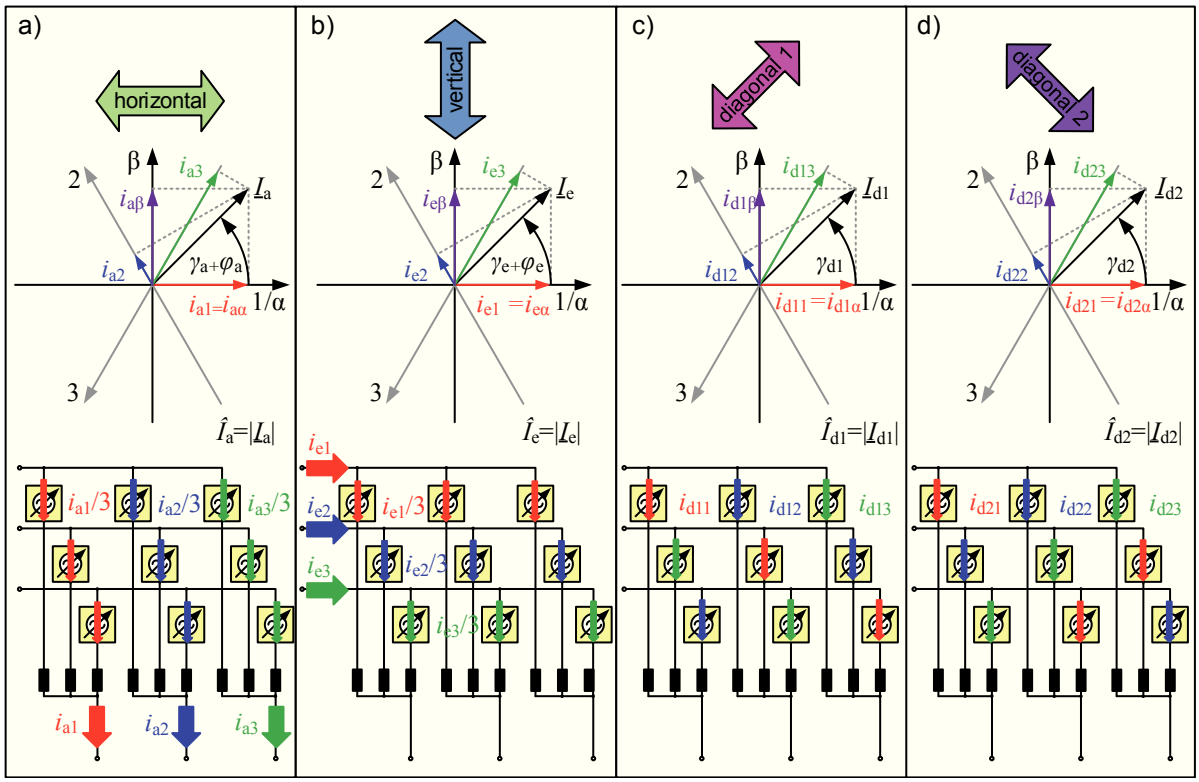

Fig. 2: Four space vectors calculated from the nine arm currents i_{xy} [2] with their distribution along the nine converter arms: a) output current space vector $\underline{I}_{\mathrm{a}}$, b) input current space vector $\underline{I}_{\mathrm{e}}$, c) diagonal current 1 space vector $\underline{I}_{\mathrm{d1}}$, d) diagonal current 2 space vector $\underline{I}_{\mathrm{d2}}$

Fig. 1b) shows the normalized arm current composition $\hat{I}_{xy}$ for an M3C feeding a 3AC machine that is operating with $\cos(\varphi_{\mathrm{a}}) = 1$. The output current component $\hat{I}_{\mathrm{a,max}}$ is doubled at standstill, compared to the nominal output current $\hat{I}_{\mathrm{a,n}}$ reached at the nominal operation point $|\nu_{\mathrm{n}}| = 0.4 = \frac{|\omega_{a,n}|}{\omega_e}$ (ν = frequency transfer ratio, ω_{a} = output angular frequency, ω_{e} = input angular frequency) [1]. This special feature of the M3C can be used to overcome high breakaway torques without over-sizing of the cell semiconductors and capacitors C_{xyz}. Experimental results using the output current overload capability are shown in Section 5.

3. Energy balancing of the Modular Multilevel Matrix Converter

One main task for the control of the M3C is to ensure that the average values of the nine arm capacitor voltages $\overline{u}_{\mathrm{C}xy}$ can be maintained at their reference values [2, 3, 4, 5]. The actual arm capacitor voltages $u_{\mathrm{C}xy} = \sum_{z=1}^{N} u_{\mathrm{C}xyz}$ contain a time-variant part $\tilde{u}_{\mathrm{C}xy}$ which depends on the energy pulsation $\tilde{w}_{\mathrm{C}xy}$ caused by the actual arm power $p_{xy} = u_{xy} \cdot i_{xy}$ [2]:

$$u_{\mathrm{C}xy} = \tilde{u}_{\mathrm{C}xy} + \overline{u}_{\mathrm{C}xy} \approx \frac{N}{C_{xyz} \cdot \overline{u}_{\mathrm{C}xy}} \int p_{xy}\mathrm{d}t + \overline{u}_{\mathrm{C}xy} = \frac{N}{C_{xyz} \cdot \overline{u}_{\mathrm{C}xy}} \int u_{xy} i_{xy}\mathrm{d}t + \overline{u}_{\mathrm{C}xy} \qquad (4)$$

To maintain a constant average arm capacitor voltage $\overline{u}_{\mathrm{C}xy}$, the control system has to ensure that the average arm power $\overline{p}_{xy}$ is zero for all nine converter arms. For this purpose a cascaded vector control system can be used [2, 3, 4, 5].

One special challenge is the operation of the M3C in cases where the input and output frequency are close together or equal $|\omega_{\mathrm{a}}| \approx |\omega_{\mathrm{e}}|$. Here some converter arms will be continuously

charged and others continuously discharged. To allow a continuous operation, the energy must be redistributed between the nine converter arms. For this purpose a zero sequence voltage u_0 together with the internal diagonal currents i_{d1} or i_{d2} can be used [2, 4, 5]. Experimental results which include the switch over to normal operation with $|\omega_{\mathrm{a}}| \neq |\omega_{\mathrm{e}}|$ are shown in Section 5.

4. Low voltage M3C laboratory prototype with 5 cells per arm

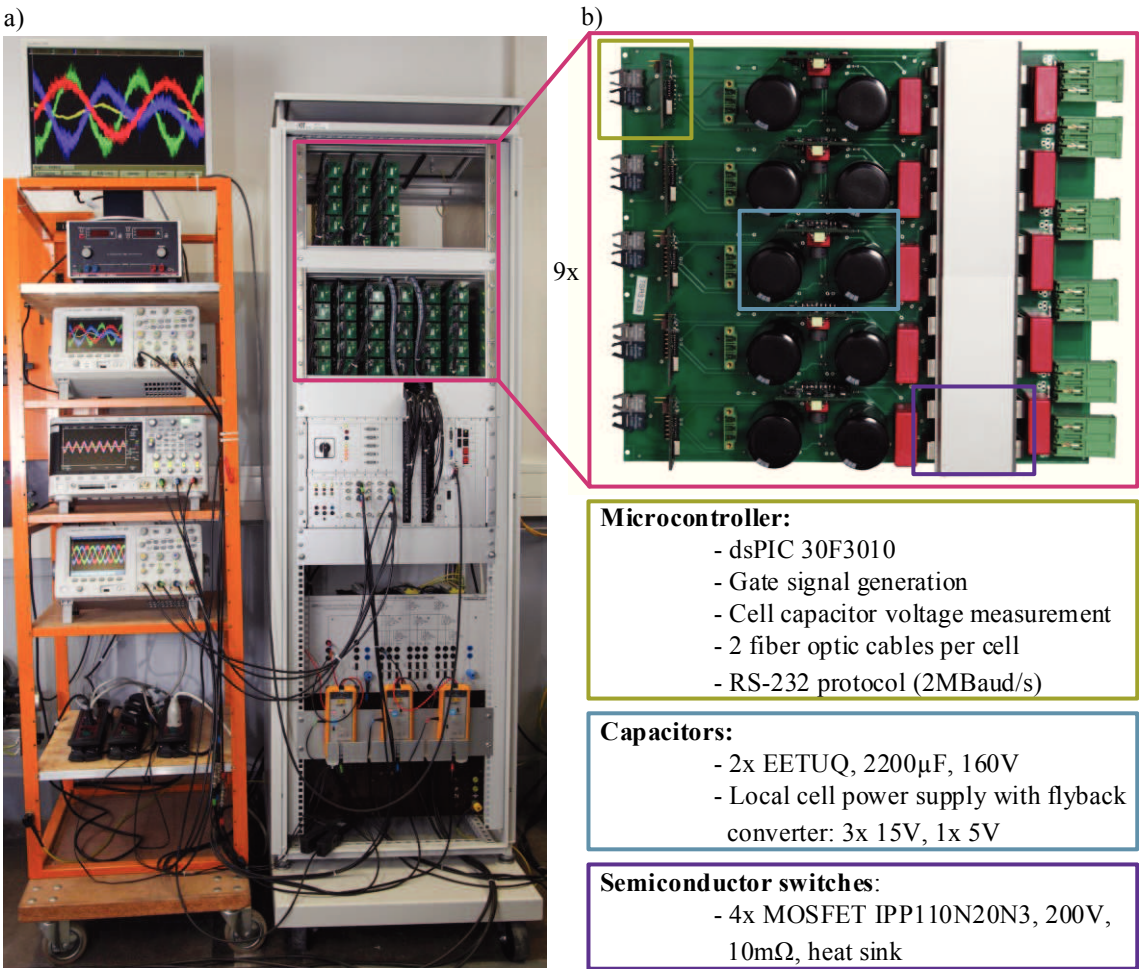

Fig. 3: a) M3C low voltage laboratory prototype with a rated power of $P_{\mathrm{n}} = 15\,\mathrm{kW}$. b) Arm circuit board with $N = 5$ cells and corresponding technical data.

Fig. 3 shows the constructed M3C low voltage laboratory prototype with a rated power of $P_{\mathrm{n}} = 15\,\mathrm{kW}$. It contains $9 \cdot 5 = 45$ cells consisting of a MOSFET H-bridge and an electrolytic capacitor. A dsPIC 30F3010 microcontroller from Microchip is used in each cell to generate the gate signals and to measure the cell capacitor voltage $u_{\mathrm{C}xyz}$. The required voltages for the cell control system are generated locally from the cell capacitor with a flyback converter. A Cyclone III Field Programmable Gate Array (FPGA) from Altera and a TMS320C6748 digital signal processor (DSP) from Texas Instruments are used as central control system. The FPGA communicates with the cell microcontrollers via 2 fiber optic cables and a RS-232 protocol. Additionally, it calculates the nine arm capacitor voltages $u_{\mathrm{C}xy}$ from the measured cell capacitor voltages $u_{\mathrm{C}xyz}$ and performs the cell balancing inside of the nine converter arms [6]. The pulse

width modulation frequency is selected to $f_{\mathrm{PWM}} = 8\,\mathrm{kHz}$. Due to the cell balancing, an average cell switching frequency of $f_{\mathrm{s}} \approx 2\,\mathrm{kHz}$ is achieved. The cascaded vector control scheme [2, 3, 6] is calculated in real time on the DSP in less than $t_{\mathrm{A}} = \frac{1}{f_{\mathrm{PWM}}} = 125\,\mu\mathrm{s}$.

5. Experimental results with a low voltage laboratory prototype

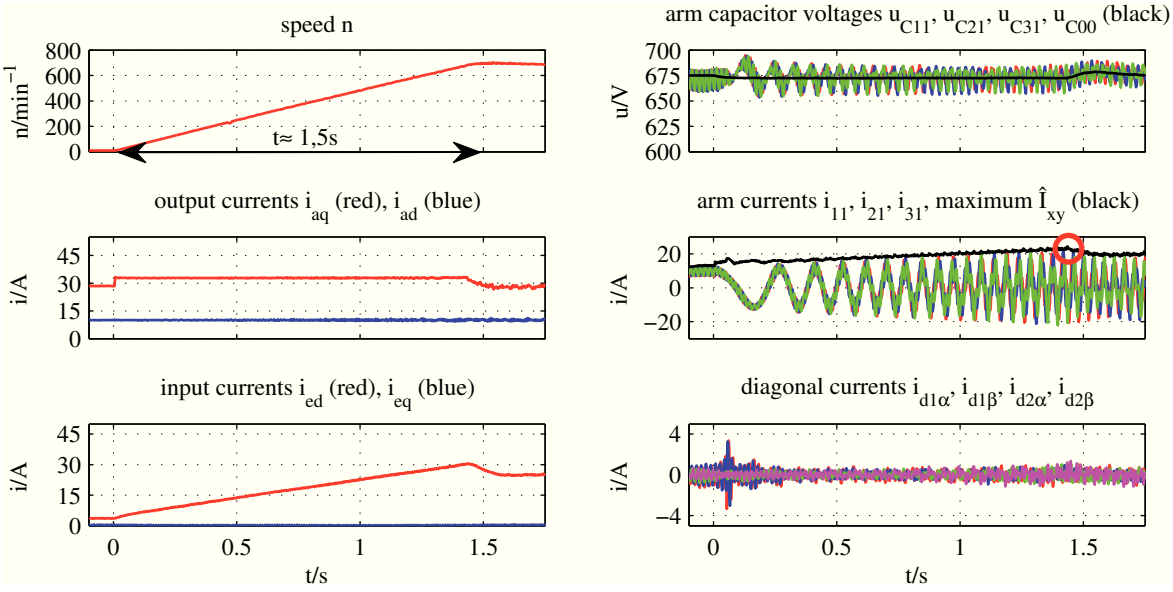

Fig. 4: Measurement of the M3C control variables during the run-up of an induction machine to $\mathrm{n} = 680\,\mathrm{min}^{-1}$ with $i_{\mathrm{aq}} \approx 32\,\mathrm{A}$, short time averaged values at $t_{\mathrm{A}} = \frac{1}{f_{\mathrm{PWM}}} = \frac{1}{8\,\mathrm{kHz}}$.

Fig. 4 shows the start up performance of the M3C feeding an induction machine up to its rated speed of $\mathrm{n} = 680\,\mathrm{min}^{-1}$ which corresponds to an electrical output frequency of $f_{\mathrm{a}} \approx 24\,\mathrm{Hz}$. The load torque $M_{\mathrm{L}} = 120\,\mathrm{Nm}$, generated by a DC-machine, is constant and corresponds to the rated torque of the induction machine and a torque generating current of $i_{\mathrm{aq}} \approx 28,5\,\mathrm{A}$. The magnetization current $i_{\mathrm{ad}} = 10\,\mathrm{A}$ and the torque generating current $i_{\mathrm{aq}} \approx 33\,\mathrm{A}$ are constant during the run-up. The run-up time is $t \approx 1,5\,\mathrm{s}$ and the maximum arm current $\hat{I}_{xy} \approx 23\,\mathrm{A}$ is reached at the end of the run-up (see red circle in Fig. 4). The active output power at that point is $P_a \approx 12\,\mathrm{kW}$. The internal diagonal currents $i_{\mathrm{d1}\alpha/\beta}$ and $i_{\mathrm{d2}\alpha/\beta}$ are small and the arm capacitor voltages $u_{\mathrm{C}xy}$ are pulsating around the actual average arm capacitor voltage $u_{\mathrm{C00}} \approx 675\,\mathrm{V}$.

The run-up time can be shortened to $t \approx 0,6\,\mathrm{s}$ by using the maximum arm current $\hat{I}_{xy} \approx 23\,\mathrm{A}$ during the entire run-up sequence, see Fig. 5. Here the torque generating current can be increased up to $i_{\mathrm{aq}} \approx 48\,\mathrm{A}$ in the low speed range resulting in a higher starting torque.

In addition it is possible to use the higher torque generating current i_{aq} in the low speed range to overcome breakaway torques. This is shown in Fig. 6. Here the initial load torque is $M_{\mathrm{L0}} = 170\,\mathrm{Nm}$ which is decreased to $M_{\mathrm{L}} = 120\,\mathrm{Nm}$ at a speed of $\mathrm{n} = 200\,\mathrm{min}^{-1}$. The M3C is able to run-up to $\mathrm{n} = 680\,\mathrm{min}^{-1}$ in about $t \approx 0,9\,\mathrm{s}$ against the initial torque M_{L0}. The initial torque generating current at standstill is $i_{\mathrm{aq,0}} \approx 38\,\mathrm{A}$ (blue circle). It is higher than the torque generating current at the end of the run-up $i_{\mathrm{aq}} \approx 33\,\mathrm{A}$ (green circle). In this case the run-up to $\mathrm{n} = 680\,\mathrm{min}^{-1}$ is only possible by using the entire arm current $\hat{I}_{xy} \approx 23\,\mathrm{A}$ to generate a higher torque generating current i_{aq} at low speeds.

Fig. 7 shows an induction machine run-up from $\mathrm{n} = 1100\,\mathrm{min}^{-1}$ to $\mathrm{n} = 1650\,\mathrm{min}^{-1}$. In the

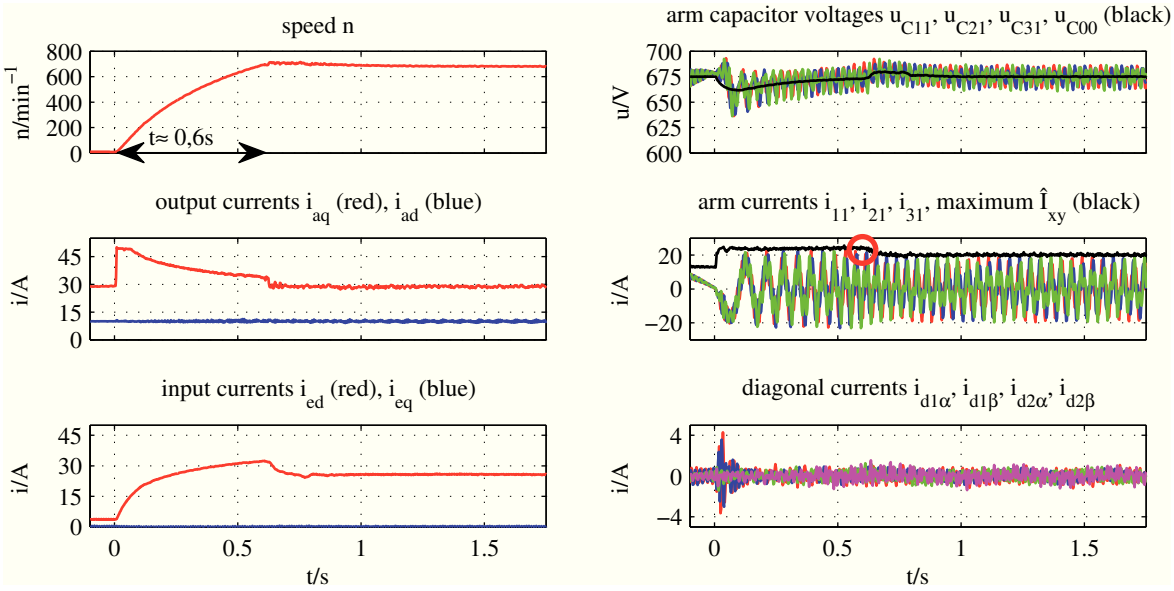

Fig. 5: Measurement of the M3C control variables during the run-up of an induction machine to $\mathrm{n} = 680\,\mathrm{min}^{-1}$ with $\hat{I}_{xy} \approx 23\,\mathrm{A}$, short time averaged values at $t_\mathrm{A} = \frac{1}{f_\mathrm{PWM}} = \frac{1}{8\,\mathrm{kHz}}$.

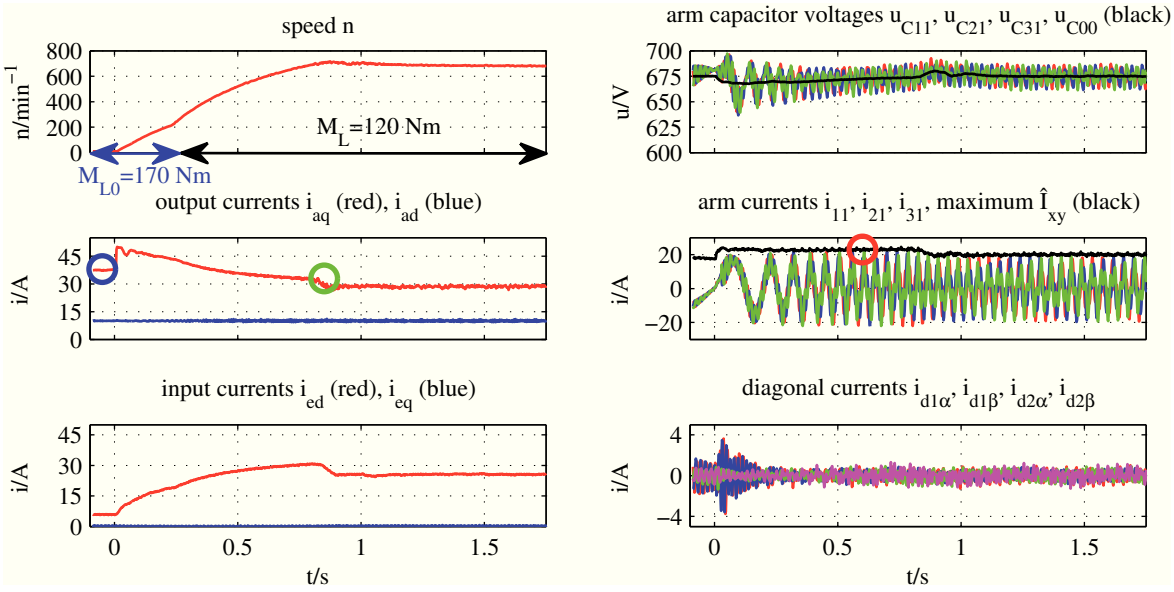

Fig. 6: Measurement of the M3C control variables during the run-up of an induction machine to $\mathrm{n} = 680\,\mathrm{min}^{-1}$ with $\hat{I}_{xy} \approx 23\,\mathrm{A}$ and a initial load torque of $M_\mathrm{L0} = 170\,\mathrm{Nm}$, short time averaged values at $t_\mathrm{A} = \frac{1}{f_\mathrm{PWM}} = \frac{1}{8\,\mathrm{kHz}}$.

frequency range $f_\mathrm{a} = 44..56\,\mathrm{Hz}$, a DC zero sequence voltage $u_0 = 90\,\mathrm{V}$ is used together with $i_{\mathrm{d1}\alpha/\beta}$ and $i_{\mathrm{d2}\alpha/\beta}$ to balance the nine arm capacitor voltages $u_{\mathrm{C}xy}$ [2, 4, 5]. The maximum arm current $\hat{I}_{xy}$ is significantly increased and reduces the maximum output currents and therefore the maximum torque. With the control strategies presented in [2, 4, 5] it is possible to achieve an active output power of $P_\mathrm{a} \approx 8.5\,\mathrm{kW}$ at $f_\mathrm{a} \approx 50\,\mathrm{Hz}$. This is more than 50% of the nominal value $P_\mathrm{n} = 15\,\mathrm{kW}$. Therefore the M3C is suitable for applications with nominal output frequencies greater than the input frequencies $|f_\mathrm{a,n}| > |f_\mathrm{e}|$ and a quadratic load characteristic. Here a successful run-up can be performed by using the control strategies presented in [2, 4, 5].

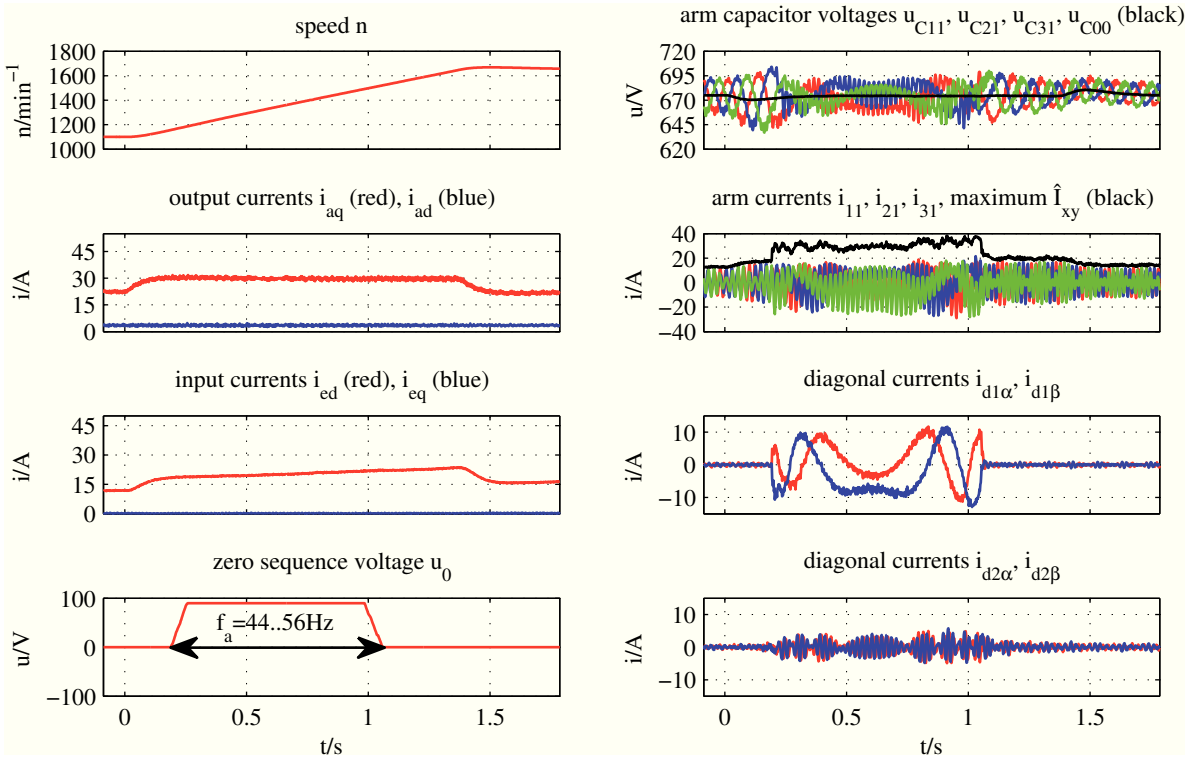

Fig. 7: Measurement of the M3C control variables during the run-up of an induction machine from $\mathrm{n} = 1100\,\mathrm{min}^{-1}$ to $\mathrm{n} = 1650\,\mathrm{min}^{-1}$, short time averaged values at $t_\mathrm{A} = \frac{1}{f_\mathrm{PWM}} = \frac{1}{8\,\mathrm{kHz}}$.

6. Applications for the Modular Multilevel Matrix Converter

The M3C is suitable for medium and high voltage applications with different input and output frequencies. It can be used for:

- Replacement of line commutated cycloconverters or conventional two or three level converters in low speed applications like direct driven wind generators or mills. In mills the output current overload capability can be used to overcome breakaway torques [1].
- Feeding the rotor circuit of Doubly Fed Induction Generators (DFIG) used for wind turbines or variable speed pump storage power plants. Here the dynamics and part load efficiency can be increased compared to fixed speed synchronous generators [7].
- Connection of offshore wind-farms via a low frequency AC grid (e.g. $16,7\,\mathrm{Hz}$) to the conventional $50/60\,\mathrm{Hz}$ public grid instead of a expensive HVDC connection [8].
- High speed drives with a quadratic load characteristic, e.g. pumps, fans, etc. Here the M3C requires smaller cell capacitors C_{xyz} compared to the Modular Multilevel Converter [9].

7. Conclusion

This paper demonstrates the operating performance of the Modular Multilevel Matrix Converter (M3C) in drive applications by using a low voltage laboratory prototype. Measurement results show the excellent run-up performance against a high breakaway torque near standstill. There-

fore the M3C is a favorable solution for applications with high torque requirements and low nominal output frequencies like mills. For applications that require higher output frequencies the run-up must be guaranteed. For this purpose the performance with equal input and output frequency is demonstrated, here more than 50% of the nominal output power can be achieved. This makes the M3C a favorable solution for medium and high voltage applications with different input and output frequencies.

Acknowledgment

The authors would like to thank the DFG (German Research Foundation) which finances this research project under grant BR 1780/8-1.

8. References

[1] F. Kammerer, M. Gommeringer, J. Kolb, and M. Braun. Overload capability of the modular multilevel matrix converter for feeding high torque low speed drives. In *Proceedings of PCIM South America , Sao Paulo, Brasil*, volume 1, pages 20–27, October 2014.

[2] F. Kammerer, M. Gommeringer, J. Kolb, and M. Braun. Energy balancing of the modular multilevel matrix converter based on a new transformed arm power analysis. In *Power Electronics and Applications (EPE'14-ECCE Europe), 2014 16th European Conference on*, pages 1–10, August 2014.

[3] F. Kammerer, J. Kolb, and M. Braun. Fully decoupled current control and energy balancing of the modular multilevel matrix converter. In *Power Electronics and Motion Control Conference (EPE/PEMC), 2012 15th International*, pages LS2a.3–1–LS2a.3–8, September 2012.

[4] W. Kawamura, M. Hagiwara, and H. Akagi. Control and experiment of a modular multilevel cascade converter based on triple-star bridge cells (mmcc-tsbc). *Industry Applications, IEEE Transactions on*, PP(99):1–1, 2014.

[5] W. Kawamura, M. Hagiwara, and H. Akagi. Control and experiment of a 380-v, 15-kw motor drive using modular multilevel cascade converter based on triple-star bridge cells (mmcc-tsbc). In *Power Electronics Conference (IPEC-Hiroshima 2014 - ECCE-ASIA), 2014 International*, pages 3742–3749, May 2014.

[6] F. Kammerer, J. Kolb, and M. Braun. A novel cascaded vector control scheme for the modular multilevel matrix converter. In *IECON 2011 - 37th Annual Conference on IEEE Industrial Electronics Society*, pages 1097–1102, November 2011.

[7] F. Kammerer, M. Gommeringer, J. Kolb, and M. Braun. Benefits of operating doubly fed induction generators by modular multilevel matrix converters. *PCIM Europe, Nuremberg, Germany*, 2013.

[8] W. Fischer, R. Braun, and I. Erlich. Low frequency high voltage offshore grid for transmission of renewable power. In *Innovative Smart Grid Technologies (ISGT Europe), 2012 3rd IEEE PES International Conference and Exhibition on*, pages 1–6, October 2012.

[9] K. Ilves, L. Bessegato, and S. Norrga. Comparison of cascaded multilevel converter topologies for ac/ac conversion. In *Power Electronics Conference (IPEC-Hiroshima 2014 - ECCE-ASIA), 2014 International*, pages 1087–1094, May 2014.